



Experimental study of ethylene counterflow diffusion flames perturbed by trace amounts of jet fuel and jet fuel surrogates under incipiently sooting conditions

Saeed Jahangirian^{a,1}, Charles S. McEnally^b, Alessandro Gomez^{a,*}

^a Department of Mechanical Engineering, Yale Center for Combustion Studies, New Haven, CT 06477, USA

^b Department of Chemical Engineering, Yale Center for Combustion Studies, New Haven, CT 06477, USA

ARTICLE INFO

Article history:

Received 18 December 2008

Received in revised form 1 March 2009

Accepted 4 March 2009

Available online 18 May 2009

Keywords:

Soot

Aromatics

Diffusion flame

Jet fuel

JP-8

Surrogate

ABSTRACT

The structure of an ethylene counterflow diffusion flame doped with 2000 ppm on a molar basis of either jet fuel or two jet fuel surrogates is studied under incipient sooting conditions. The doped flames have identical stoichiometric mixture fractions ($z_f = 0.18$) and strain rates ($a = 92 \text{ s}^{-1}$), resulting in a well-defined and fixed temperature/time history for all of the flames. Gas samples are extracted from the flame with quartz microprobes for subsequent GC/MS analysis. Profiles of critical fuel decomposition products and soot precursors, such as benzene and toluene, are compared.

The data for C7–C12 alkanes are consistent with typical decomposition of large alkanes with both surrogates showing good qualitative agreement with jet fuel in their pyrolysis trends. Olefins are formed as the fuel alkanes decompose, with agreement between the surrogates and jet fuel that improves for small alkenes, probably because of an increase in kinetic pathways which makes the specifics of the alkane structure less important.

Good agreement between jet fuel and the surrogates is found with respect to critical soot precursors such as benzene and toluene. Although the six-component Utah/Yale surrogate performs better than the Aachen surrogate, the latter performs adequately and retains the advantage of simplicity, since it consists of only two components.

The acetylene profiles present a unique multimodal behavior that can be attributed to acetylene's participation in early stages of formation of soot precursors, such as benzene and other large pyrolysis products, as well as in the surface growth of soot particles.

© 2009 The Combustion Institute. Published by Elsevier Inc. All rights reserved.

1. Introduction

Transportation fuels, including jet fuels, constitute a significant share of the world's energy consumption. Common jet fuels include Jet A-1, Jet A, and JP-8. They comprise hundreds of aromatic compounds and aliphatic components, such as straight chain paraffins, branched chain paraffins, cycloparaffins, and alkenes [1]. Depending on the source of the parent crude and the refinery process, their composition may vary significantly. The future fuel supply will become more and more diversified and burning a broad range of fuels as well as reduction of pollutant (e.g., soot) formation will pose new challenges to the implementation of their combustion. This trend will necessitate fundamental studies in well-defined and well-controlled environments to establish, among

other aspects, the chemical kinetic behavior of these complex fuel blends.

Characterization and simulation of jet fuel chemical kinetics and transport is only practical by identifying surrogate mixtures having a relatively small number of components. Colket et al. [2] proposed a road map for future development of surrogate fuels, which resulted from discussions at a number of meetings of a surrogate fuel working group. The surrogate physical and chemical properties should capture essential features of real fuels in prototypical combustion conditions. Surrogate mixtures have been defined and tested in many experimental conditions and configurations, including flow/stirred reactors, shock tubes, premixed flames, pool fires, and counterflow diffusion flames. A comprehensive review was presented by Dagaut et al. [3]. In the late 1980s, Wood et al. [4] formulated a 14-component JP-4 surrogate based on its compound class composition and distillation curves. Subsequent efforts by Schulz et al. [5] led to a 12-component jet fuel surrogate. Feasibility, simplicity, fuel class similarity, and cost are essential criteria that guided subsequent work aimed at decreasing the number of components to produce more manageable formulations. Violi et al. [6] reported a six-component Utah surrogate de-

* Corresponding author. Address: Department of Mechanical Engineering, Yale University, P.O. Box 208286, New Haven, CT 06520-8286, USA. Fax: +1 203 432 7654.

E-mail address: alessandro.gomez@yale.edu (A. Gomez).

¹ Present address: Department of Mechanical Engineering, Michigan State University, East Lansing, MI 48824, USA.

signed to match the volatility of jet fuel and its overall sooting behavior based on smoke point tests. More recently, the number of components has further decreased [7–9], with the minimization effort culminating in the two-component Aachen surrogate [10]. Single-component surrogates, though initially contemplated, are now generally thought to lack the necessary flexibility to match the jet fuel performance in a sufficiently broad parameter space. In recent work in pressurized flow reactors, Natelson et al. [11] experimentally studied jet fuel and a three-component jet fuel surrogate suggested by the surrogate fuels working group at pressures as high as 0.8 MPa. The three-component surrogate showed higher reactivity than jet fuel suggesting that an improvement is possible by adding iso-paraffins. Experiments by Holley et al. [12] in a counterflow non-premixed configuration found that the six-component Utah surrogate [6] increased ignition propensity and resistance to extinction compared to jet fuel. This behavior was attributed to mismatched transport properties. Vasu et al. [13] measured ignition delay times of jet fuels in a shock tube and compared them with predictions of some current kinetic mechanisms [14,15]. The five-component Utah surrogate (Violi Surrogate #3 [6]), when used with the Milan mechanism [14], revealed the closest agreement in ignition delay times, especially in capturing the high-temperature trend. This work has continued on individual components of the surrogate mixture, *n*-dodecane ($n\text{-C}_{12}\text{H}_{26}$) and methylcyclohexane (MCH), with shock-tube experiments on the former [16] and with measurements of OH time-histories of oxidation behind reflected shocks for the latter [17].

In our earlier study at Yale [18], good agreement was reported for extinction strain rate and temperature profiles between jet fuel and a six-component surrogate in *non-sooting* counterflow diffusion flames. This contribution began in collaboration with the research groups at University of Utah and University of Milan, with the Utah group establishing the surrogate mixture formulation and the Milan group developing the chemical kinetic model for this surrogate including 221 species and 5032 reactions [18]. The formulation used in [18] and in all subsequent work at Yale departs slightly from the Utah surrogate in that the vol% composition of the six components (Surrogate #1) in Violi et al. [6] was reinterpreted as molar fractions, which resulted in relative average changes of 27% in the component molar compositions. We shall refer to this surrogate, whose composition is specified in Table 1 below, as the Utah/Yale surrogate. More detailed investigations followed in our laboratory, with the chemical analysis of the structure of a methane counterflow diffusion flame perturbed with thousands of ppm of either jet fuel or the six-component jet fuel surrogate [19,20] in highly diluted and *non-sooting* flames, including detailed one-dimensional modeling using the Milan mechanism. The surrogate captured the general jet fuel behavior reasonably well except for ethylene and small aromatics such as benzene and toluene. The discrepancy in aromatics is cause for concern, if confirmed under sooting conditions, since aromatics are critical precursors to soot.

The sooting behavior of jet fuels, especially at take-off, is an issue in most aero-turbines for which non-premixed configurations are preferred. Therefore, any surrogate formulation needs to be validated with respect to this performance. Gas sampling is problematic in the presence of large amounts of soot because of the inevitable clogging of the microprobe orifice. This problem can be circumvented if conditions of *incipient sooting* are chosen, in which the soot loading is kept at the minimum necessary to discern a faint blackbody luminosity in the flame. These are the conditions chosen in the present study.

A comprehensive investigation is conducted on the detailed flame structure of ethylene counterflow diffusion flames perturbed by trace amounts (2000 ppm, molar) of jet fuel and two surrogates via gas sampling and chemical analysis. The ultimate goal is to

ascertain if the surrogate formulations are reasonably successful in mimicking the performance of jet fuel, especially with respect to the behavior of small aromatics for which discrepancies were observed under non-sooting conditions [19,20]. Two surrogates are examined: the six-component Utah/Yale surrogate used in all previous work in our laboratory [18–20], and a two-component Aachen surrogate, that has been reported to mimic not only conditions of extinction and autoignition, but also to match the soot volume fraction behavior, especially under relatively high strain rates [10]. Semi-detailed chemical kinetic mechanisms are available for both surrogates [10,21,22].

2. Experimental setup

Fig. 1 shows a schematic of the experimental setup. It consists of a counter-flow burner [19], including a nitrogen shroud that shields the flame from room drafts and ensures burning in the controlled atmosphere that is determined by the composition of the feed streams. The inner diameter of the fuel and oxidizer outlets is 12.5 mm and the burner separation is 14.1 mm. Slightly nitrogen-diluted air is used as the oxidizer while the fuel is nitrogen-diluted ethylene doped with either jet fuel or the surrogates. To ensure complete vaporization of the dopant liquid, an electro-spray operated in the multi-jet mode [23] disperses the liquid fuel in the preheated fuel/nitrogen stream. This approach provides flexibility in flow rates without compromising the stability of the flame. To prevent condensation downstream of the electro-spray unit, PID controllers keep the fuel line at 430 K, which is well above the dew point of the dopant/ $\text{C}_2\text{H}_4/\text{N}_2$ mixtures. Gas samples are extracted from the flame through a microprobe, consisting of a small silica probe with an outer diameter of 340 μm and an inner diameter of 170 μm . Details of the different microprobes used previously can be found in [19,20].

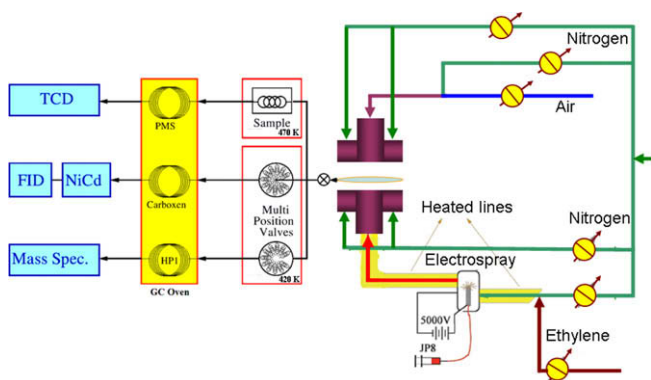
The chemical analysis is performed by a gas chromatograph (Agilent 6890A) equipped with mass spectrometer (MSD, Agilent 5973N), thermal conductivity (TCD), and flame ionization (FID) detectors. The instrument is capable of quantifying complex hydrocarbon mixtures, CO, CO_2 , O_2 , and N_2 . It uses two capillary columns, a Supelco Carboxen and an Agilent HP-1, connected to the FID and MSD, respectively. In addition, the TCD measures non-hydrocarbon stable gases separated by means of a third column (Alltech, Packed Molecular Sieve). Because of its much wider linear range, this detector is better suited than the MSD for the analysis of gases present as large fractions of the gas sample and/or in greatly varying amounts, e.g., N_2 and O_2 . A homemade nickel-based catalytic converter (Methanizer) allows for FID quantification of CO and CO_2 upon their conversion into methane in the presence of hydrogen. The system can separate and quantify H_2 , N_2 , O_2 , CO, CO_2 , light gaseous hydrocarbons, and higher hydrocarbons up to at least C14.

Species are identified during the GC/MS data post-processing by both the column retention time and the molecule-specific mass spectrum. GC/MS analysis produces a wealth of information, but has one main drawback: it takes a very long time to perform a flame scan. At the small liquid flow rates of interest for jet fuel (e.g., 1.6 ml/h), a syringe pump is used to deliver the fuel. Preserving a steady flame over the analysis time, which is on the order of one day, would be challenging: it would require repeated flame shut-offs for reloading of the syringes. Thermal transients would affect boundary conditions, and other inevitable consequences such as sampling probe distortions might cause reproducibility problems that affect the self-consistency of the data. To sidestep these problems, a semi-automated chemical analysis method is employed that consists of sampling the gas and storing it in a battery of sampling loops using two pneumatic-actuated injection

Table 1
Boundary conditions.

		Flame A Baseline	Flame A* Equal carbon	Flame B Jet fuel	Flame C Utah/Yale surrogate	Flame D Aachen surrogate
Fuel side	Molar composition					
	N ₂	0.7278	0.7280	0.7340	0.7339	0.7339
	C ₂ H ₄	0.2722	0.2719	0.2641	0.2641	0.2641
	C2 (ethane) impurities	637 ppm	636 ppm	618 ppm	618 ppm	618 ppm
	Jet fuel ^a (C ₁₁ H ₂₁)			1953 ppm		
	Methyl-cyclohexane				394 ppm	
	Iso-octane				197 ppm	
	<i>m</i> -Xylene				295 ppm	
	Tetralin				98 ppm	
	<i>n</i> -Dodecane				591 ppm	
	<i>n</i> -Tetradecane				394 ppm	
	Total				1970 ppm	
	1,2,4-Trimethylbenzene					450 ppm
	<i>n</i> -Decane					1520 ppm
	Total					1970 ppm
Mass flux (g/(cm ² min))	1.619	1.683	1.684	1.683	1.682	
Temperature (K)	407	407	407	407	407	
Oxidizer side	Molar composition					
	N ₂	0.8070	0.8070	0.8070	0.8070	0.8070
	O ₂	0.1843	0.1843	0.1843	0.1843	0.1843
	Mass flux (g/(cm ² min))	1.891	1.925	1.925	1.925	1.925
	Temperature (K)	370	370	370	370	370
	Strain rate (s ⁻¹)	89.9	85.2	92.3	92.3	92.3
	Z _f	0.18	0.18	0.18	0.18	0.18

^a The jet fuel was provided by WPAFB (POSF No. 4658). The composition of this “average” jet fuel blend in vol% is: 55.2% paraffins (*n*- and *i*-), 17.2% monocycloparaffins, 12.7% alkyl benzenes, 7.8% dicycloparaffins, and 4.9% indans and tetralin. The balance, ≈2%, is in naphthalenes and tricycloparaffins.

**Fig. 1.** Schematic of the experimental setup.

valves and two multi-position valves, as shown in Fig. 1 [11,19,20,24,25]. One of the pneumatic injection valves is responsible for the TCD analysis (top left in the figure) that is executed in real time, since it requires about 2 min per data point. The other valve controls the FID and the MS. Since these two instruments require a much longer time to complete a measurement, the samples are stored in two sets of 16 sample loops using two multi-position valves (Valco[®]) and analyzed overnight by a computer-automated sequence. An optimized time–temperature program for the chromatographic columns keeps the total analysis time at a minimum and ensures that aging of samples does not change the sample concentrations significantly.

Temperature measurements are performed using flame-welded, silica coated Pt–10%Rh/Pt thermocouples with a typical junction diameter measuring on the order of 70 μm. Standard corrections for radiative losses are applied. In some temperature measurements, a gas sample probe is also placed within the flame to assess the probe’s intrusiveness. As a result, any spatial offset between temperature and species profiles would be mostly due to the sampling probe intrusiveness. Temperatures of both feed

streams at the burner outlets are measured by a K-type thermocouple.

Accuracy in the GC/MS analysis and reproducibility of the data were ensured by analyzing gas mixtures of known composition (Scotty[®]) and repeated sampling at the same position in the flame. Standard calibration gases (Scotty[®]) are used for calibration of light gaseous species. Aliquots of liquid hydrocarbons dissolved in acetone are injected into the GC/MS for the calibration of heavy liquid hydrocarbons. The total error is estimated at 7% for light species and 12–15% for the heavier ones.

3. Criterion for flame comparison

The advantages of doping a baseline flame with trace amounts of prevaporized liquid fuel were mentioned in our previous studies [19,20]. This approach was first employed in non-premixed flames by Hamins et al. [26] and has been more extensively used by McEnally and Pfefferle [27,28]. This approach minimizes the potential for vapor condensation since the condensable species is at very small concentrations. The temperature–time history can be easily adjusted to be identical for all flames, so that this counterflow flame environment can be regarded as a flow reactor in which the residence time and the temperature profile are adjusted by varying the strain rate and the feed stream composition, respectively. The temporal history is identical since the flames have essentially the same mass averaged velocities at the boundaries and identical temperature profiles, which leads to the same evolution of the velocity profile via gas expansion. Furthermore, critical, non-chemical variables, such as temperature and velocity, as well as probe-induced perturbations, can be evaluated once and for all in the baseline flame.

The counterflow configuration is chosen, as in our previous studies, as the work horse for a systematic study of fuels with complex chemical kinetics and their coupling with transport in the simplest possible fluid dynamic environment: a one-dimensional laminar flow. It is amenable to detailed computational models that are now routinely applied in most combustion laboratories,

at least for simple fuels. Since our goal is to focus on conditions yielding soot formation and since soot is an issue primarily in non-premixed flame environments [28], a non-premixed counter-flow flame is appropriate for our study. For such a flame, the density corrected strain rate, a , is defined as [29]

$$a = \frac{2V_{ox}}{L} \left(1 + \frac{V_f \sqrt{\rho_f}}{V_{ox} \sqrt{\rho_{ox}}} \right), \quad (1)$$

where V_{ox} and V_f are the flow velocities normal to the stagnation plane at the oxidizer and fuel boundaries, respectively, L is the burner separation, and ρ_{ox} and ρ_f are the densities of the mixture at the oxidizer boundary and the fuel boundary, respectively. The stoichiometric mixture fraction, z_f , is defined as

$$z_f = \frac{1}{1 + s \frac{Y_{FF}}{Y_{OO}}}, \quad (2)$$

where s is the stoichiometric mass ratio of oxygen to fuel, Y_{FF} and Y_{OO} are the feed stream mass fraction of the fuel (regardless of the chemical composition) and oxygen, respectively. Our previous study [20] focused on a highly diluted methane baseline flame doped with 1000 ppm of jet fuel or a surrogate under non-sooting conditions, with $T_{max} \approx 2012$ K, $a = 144$ s⁻¹, and $z_f = 0.76$. Here we use an ethylene baseline flame, since C₂H₄ has a greater soot propensity than CH₄, so that its boundary conditions can be adjusted with ease for it to be at the onset of soot formation. To that end, the temperature/time history needs to favor soot formation, with higher temperatures and lower residence times [30–32], and the stoichiometric mixture fraction, z_f , would have to decrease sharply in comparison with our previous studies to values less than 0.5 to ensure that the flame locates itself on the oxidizer side of the stagnation plane and oxidation of soot precursors is avoided [33].

A value of $z_f = 0.18$ was chosen for all flames. The stoichiometric mass ratio of oxidizer to fuel, s , for the baseline flame is 3.42, whereas Y_{FF} and Y_{OO} are 0.27 and 0.2, respectively. Table 1 specifies the overall mean strain rate and the boundary conditions (mole fractions, total mass flux, and outlet temperatures of both fuel and oxidizer streams) for the five flames under consideration: the baseline ethylene flame, Flame A; the ethylene + jet fuel flame, Flame B; the ethylene + Utah/Yale surrogate flame, Flame C; the ethylene + Aachen surrogate flame, Flame D; and a fifth flame, Flame A*. The latter is a modified baseline ethylene flame whose total fuel carbon flux matches the doped flames. The total carbon flow rate is 3.81×10^{-2} mol/min and 3.96×10^{-2} mol/min for Flame A and Flame C, respectively. Flame A* is established by modifying the boundary conditions of Flame A to ensure the same z_f , temperature profile, and carbon molar flow rate as Flame C. To avoid clutter, the only data that will be presented for Flame A* is the concentrations of a few minor species such as aromatics. A chemical formula of C₁₁H₂₁ and density of 0.81 g/cm³ were used for jet fuel [34]. The jet fuel was provided by Wright-Patterson Air Force Base (POSF No. 4658). To account for the considerable variability in the composition of jet fuel from different refineries, an “average” jet fuel was synthesized by mixing together five Jet A fuels from different U.S. manufacturers. The composition of that blend in vol% is: 55.2% paraffins (n- and i-), 17.2% monocycloparaffins, 12.7% alkyl benzenes, 7.8% dicycloparaffins, and 4.9% indans and tetralin. The balance, $\approx 2\%$, is in naphthalenes and tricycloparaffins. The Utah/Yale surrogate is the six-component blend of well-known hydrocarbons used in our previous work [18,19], while the Aachen surrogate is a two-component surrogate as used in [10]. The surrogate components are made by mixing high purity hydrocarbons (Sigma-Aldrich $\geq 99\%$ purity). Trace amounts of an ethane impurity in the C₂H₄ supply were revealed by chromatographic analysis at about 620 ppm. The ethane impurity of each flame has been listed in Table 1.

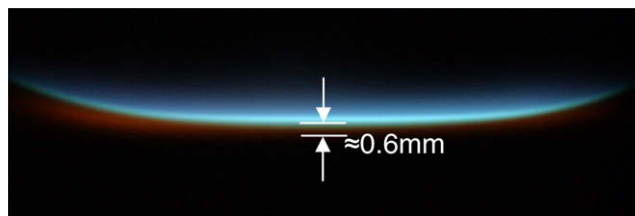


Fig. 2. Photograph of the flame at the onset of sooting. The thickness of the sooting zone with orange luminosity underneath the blue zone is about 0.6 mm.

A photograph of Flame C, the baseline flame doped with the Utah/Yale surrogate, is shown in Fig. 2. A layer of orange luminosity is visible underneath the flame chemiluminescence. The dopant concentration is chosen based on two considerations: (1) it should be sufficiently small so as not to change the overall flame structure and to preserve incipient sooting conditions, such that clogging of the microprobe orifice is avoided without resorting to special probes with attendant deterioration of the spatial resolution [35]; and (2) it should be sufficiently large so that the jet fuel/surrogate contribution to the production of critical species, such as soot precursors (e.g., small aromatics) can be discriminated from the contribution of the baseline flame. On the basis of these considerations, the ethylene flame was doped with 2000 ppm of either jet fuel or its surrogates. However, the addition of even such a small amount of these fuels increases the peak temperature by 20–30 K and the flame location shifts slightly toward the oxidizer side. To preserve the temperature–time history and ensure comparable Arrhenius kinetics among all of the flames, the temperature profile needs to be the same in all of them. Also, since the mixture fraction is a single-valued complementary error function of the axial position, fixing its value at $z_f = 0.18$ ensures that the flame position is unaltered by the perturbation. To maintain the same temperature profiles as in the baseline flame, we increased the inert mole fraction in the fuel stream, which leads to a small change in z_f and a further shift of the flame towards the oxidizer side. We compensated for this shift by a small increase in the oxidizer flow rate to move the stagnation flame in the opposite direction, towards the fuel side.

4. Results and discussion

4.1. Similarities in temperature and species profiles among flames

Fig. 3 presents a comparison between the temperature profiles of Flame A (baseline), Flame C (doped with the Utah/Yale surrogate), and Flame A* (baseline with the same carbon mole flux as Flame C). Note that the temperature profiles are indistinguishable among the three flames, which means that our strategy of establishing virtually identical temperature–time histories is successful. Since the overall jet fuel heat release behavior was indirectly validated with the Utah/Yale surrogate in [18] and with the Aachen surrogate in [10] by examining the extinction behavior and the temperature profiles of such flames, the same concentration of jet fuel and of the Aachen surrogate should lead to identical temperature histories. An additional temperature profile is shown for the baseline flame in the absence of the sampling probe. Comparison between the temperature profiles confirms an overall probe-induced perturbation that results in a 0.5-mm shift towards the fuel side, consistent with similar conclusions from planar laser induced fluorescence [20].

Fig. 4 compares some major species profiles among Flames A–D. Unless specifically noted in the subsequent figures, no experimental data of Flame A* are shown to avoid excessive cluttering of figures. Full blue symbols are used for the baseline ethylene flame

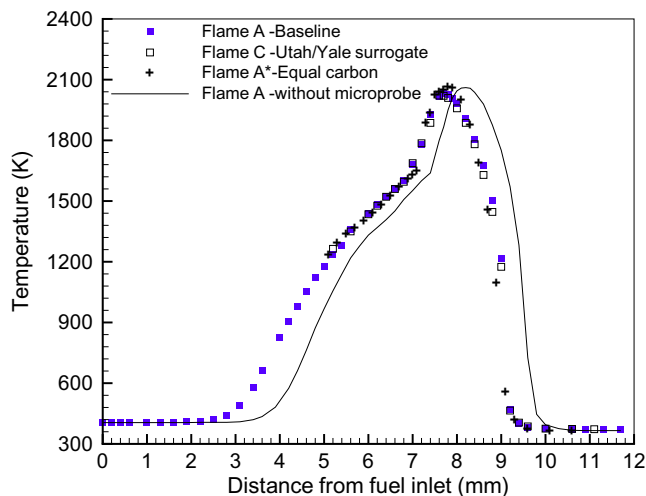


Fig. 3. Temperature profiles. Symbols: Flames A, C, and A* with microprobe in. Line: Flame A in the absence of microprobe.

(Flame A), full black symbols for the jet fuel-doped flame (Flame B), open symbols for the Utah/Yale surrogate counterpart (Flame C), full red symbols for the Aachen surrogate counterpart (Flame D), and + for the modified baseline flame (Flame A*) in this and all subsequent figures. Our goal was to perturb a well-defined baseline ethylene flame with the addition of trace amounts of jet fuel or surrogates. No distinction is observed in the profiles of the five flames with respect to CO and CO₂. O₂ was only measured in Flame A and is shown in the figure to illustrate the overall non-premixed flame structure. The profiles of C₂H₄ are also identical, except at the fuel side boundary where the mole fraction has necessarily changed between the baseline flames (Flames A and A*) and the doped flames (Flames B, C, and D) because of the flow rate adjustments discussed in Section 3. As elaborated before, the temperature profiles (Fig. 3) of these flames are virtually the same. The absence of significant changes in the concentrations of CO and CO₂ and of temperature because of the presence of either jet fuel or the surrogates indicates that these species and the heat release are produced predominantly by the oxidation of C₂H₄. The blue flame in Fig. 2 locates itself at approximately $z = 6.2$ – 6.4 mm. The thickness of the orange

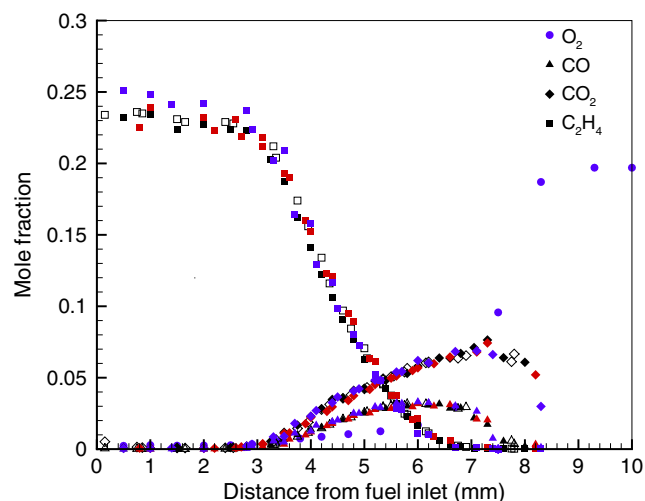


Fig. 4. Major species profiles: Flame B (full black symbols), Flame C (open symbols), Flame D (red symbols), and Flame A (blue symbols). (For interpretation of the references to color in this figure legend, the reader is referred to the web version of this article.)

sooting zone is about 0.6 mm. The asymmetry in the temperature profile is due to endothermic pyrolysis reactions between $z = 5$ and 7 mm. Detailed modeling of ethylene non-premixed flames confirms the existence of such a zone [36]. The maximum CO₂ mole fraction is slightly larger than that of the methane non-sooting flames in our previous experiments [20], whereas the peak of CO mole fraction is nearly 1.5 times larger than that of the non-sooting flames. This difference is attributable to the nitrogen mole fraction being smaller in the ethylene flames.

A drawback with probing of non-premixed flames in general is that the layer where interesting products are abundant is narrow and comparable to the spatial resolution of regular probes. The CO profiles of our sooting flames are wider than in [20]. One of the reasons for this behavior is that the strain rate of these flames is smaller than the strain rate of the non-sooting flames (the flame thickness scales inversely with \sqrt{a}). Having a wider region where chemical reactions are occurring makes the probing easier and more reliable, especially since we want to track the formation of aromatics.

Fig. 5 compares the methane mole fractions among the five flames. Methane in the present study, unlike [20], is a minor species produced by pyrolysis and oxidation of the ethylene, and of the jet fuel or surrogates in concentrations below 100 ppm. The peaks of the methane profiles for all flames are located at $z \approx 5.4$ mm. The doped flames have virtually the same methane profiles, whereas the peaks of methane mole fraction for the baseline flames (Flames A and A*) are 15% smaller. The similarity of the methane profiles, combined with the similarities in major species and temperature that were previously discussed, lends credence to our use of these flames as a sort of flow reactor with virtually identical conditions, except for the imposed perturbation.

4.2. C7–C15 alkanes

Fig. 6 shows the profiles of the C7–C15 alkanes in the doped flames, B, C, and D. Only one set of data is shown for the jet fuel-doped Flame B to avoid cluttering of the figure. The iso-octane concentration in Flame B is about 0.5 ppm and it is not shown. Most alkanes in the jet fuel-doped Flame B (Fig. 6a) disappear because of pyrolysis at $z \approx 5$ mm, except for decane, undecane, and tridecane that decay at $z \approx 5.2$ mm, and dodecane that disappears at $z \approx 5.4$ mm. In the Utah/Yale surrogate-doped Flame C, the disap-

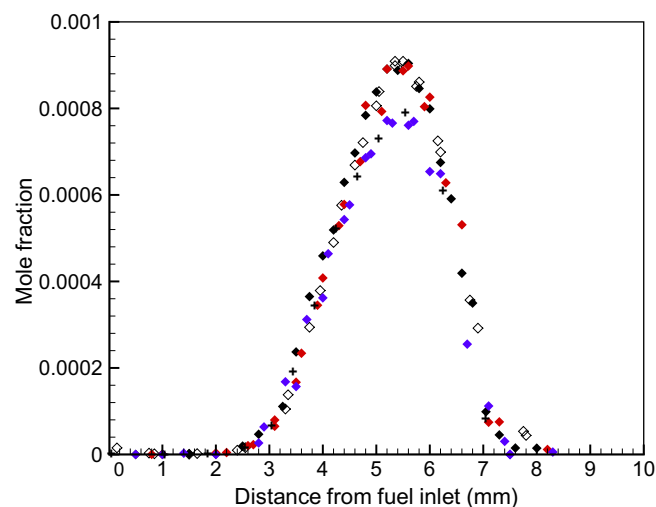


Fig. 5. Methane mole fraction profiles: Flame B (full black symbols), Flame C (open symbols), Flame D (red symbols), Flame A (blue symbols), and Flame A* (+). (For interpretation of the references to color in this figure legend, the reader is referred to the web version of this article.)

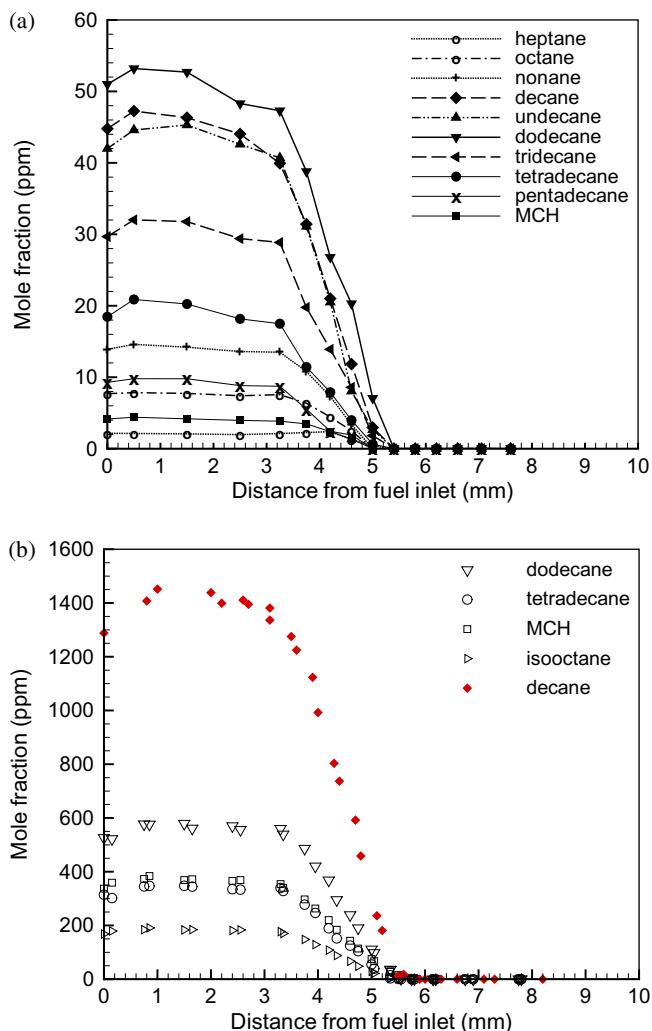


Fig. 6. Comparison of C7–C15 alkanes; (a) Flame B, (b) Flames C (open symbols), and Flame D (red symbols). (For interpretation of the references to color in this figure legend, the reader is referred to the web version of this article.)

pearance of surrogate *iso* and *normal* paraffins is delayed to nearly $z = 5.4$ – 5.5 mm. In the Aachen surrogate-doped Flame C that has only one alkane (decane), its disappearance occurs at $z \approx 5.6$ mm. The data presented here are consistent with typical decomposition of large alkanes. The observed profiles are reflective of the chemistry of jet fuel or the surrogates, since the oxidation of C_2H_4 does not yield any of these large alkanes, as also confirmed by preliminary simulations of the baseline flame with the semi-detailed Milan mechanism. Jet fuel and both surrogates show a reasonably good agreement in the pyrolysis trends of large alkanes.

Whereas the chromatograms of the surrogates are clean with distinct peaks [19] and the quantification of their components poses no difficulties, for complex fuel blends such as jet fuel that contain a large number of alkenes and alkylbenzenes having different isomers, the chromatograms are subject to interference. The quantification of these isomers is often affected by overlapping peaks from other molecules. As a result, the chromatogram, shown in Fig. 7, contains a large “grassy” background and is very hard to analyze. The reason for the modest presence of alkanes in the jet fuel-doped Flame B (Fig. 6a), despite the fact that they are known to be major components of jet fuel, is because the total alkane component is spread over many different individual alkanes. The chromatogram was measured for a gaseous sample extracted near the burner mouth, that is, before any significant chemistry had taken

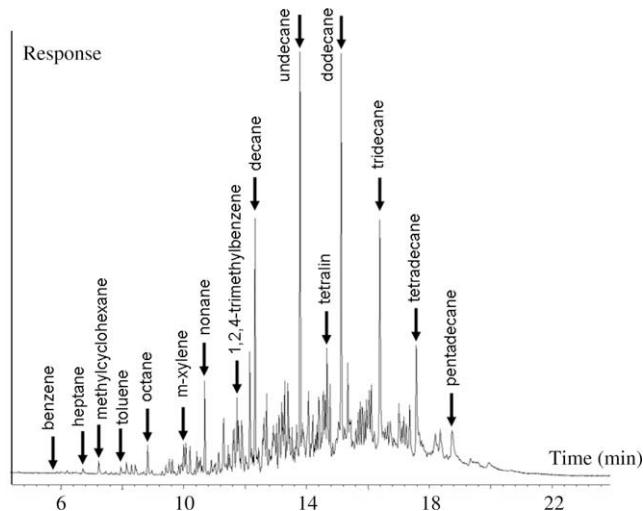


Fig. 7. Typical jet fuel MS chromatogram, as measured from a gaseous sample extracted near the burner mouth. The arrows denote compounds that were identified and quantified.

place. The final number of species we were able to measure is 33, and another 20 were correctly identified but their quantification lacks the necessary accuracy. There is a plethora of smaller, unidentified peaks and a pedestal on which the peaks are superimposed. The presence of the pedestal prevents us from performing an accurate integration for these peaks. The dominant peaks in Fig. 7 are associated with C9–C15 alkanes, whereas only a few of the smaller peaks, associated with smaller alkanes and aromatics, are marked. The quantified alkanes in Fig. 7 are regarded as tracers for a broader group of large alkanes in jet fuel. Similarly, the quantified small aromatics are indicators of a larger number of similar molecules. Therefore, the present data provide a general picture of the chemical evolution in the pyrolysis and oxidation of jet fuel in a sooting diffusion flame, with the caveat that the comparison with surrogates can only be qualitative for C7–C15 alkanes or alkenes upstream of the flame zone.

A comparative analysis of the total carbon count helps us to evaluate the GC/MS performance with respect to large hydrocarbons. For our sooting Flames B, C, and D a comparison of the total carbon counts from the liquid dopants is shown in Fig. 8. The total carbon mole fraction excludes the contributions from major products CO and CO_2 , and their primary source, C_2H_4 . Unlike a similar figure in [20], it also excludes the contributions from acetylene since, as shown in Section 4.4, the production of acetylene is mostly attributed to the ethylene portion of the fuel. Therefore, the comparison in Fig. 8 should account for all of the measured carbon in the parent liquid fuel dopant and their intermediate pyrolysis products. We measured approximately 6.4 times as much carbon at the fuel boundary in the surrogate-doped flames as in the jet fuel-doped flame. Yet, the actual carbon must be nearly the same at this location since the overall molecular weight and flow rates of the injected vapor are comparable in the three flames. The data for Flame B show a flat profile hovering around 3100 carbon ppm up to $z \approx 3.8$ mm. For Flames C and D, the total carbon count has an initial plateau around 19,000 ppm up to $z \approx 3.3$ mm, after which it monotonically decreases as CO and CO_2 are formed. This discrepancy suggests that we properly quantified only roughly 15% of the total carbon introduced as jet fuel vapor, whereas the fractions of carbon recovered from the Utah/Yale surrogate and the Aachen surrogate are roughly 93% and 92%, respectively. After $z \approx 5.4$ mm, all three profiles follow a similar quantitative trend. At about $z \approx 7.7$ mm, the oxidation of dopants is completed and no carbon persists in hydrocarbons in these flames.

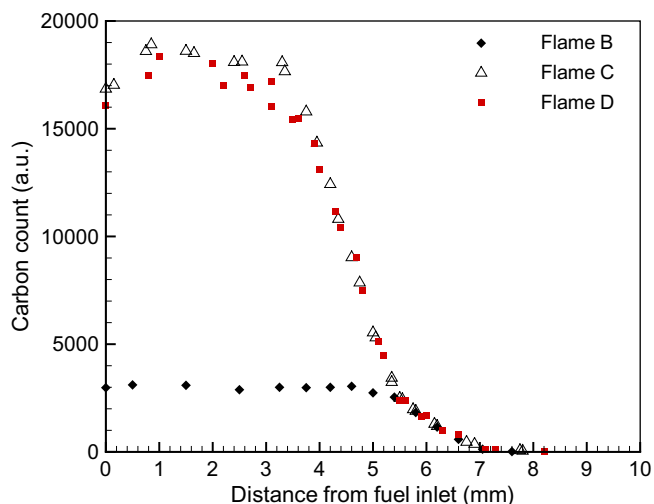


Fig. 8. Partial carbon mole fraction profiles for Flame B (full symbols), Flame C (open symbols), and Flame D (red symbols). Contributions from ethylene, CO, CO₂, acetylene, and ethane are not considered.

4.3. C3–C6 alkanes and alkenes

Fig. 9 illustrates how C5 and C6 alkenes, such as 1-pentene and 1-hexene, are formed as larger alkanes decompose in Flames A–D. There was no detectable 1-hexene in the baseline ethylene Flame A. Smaller concentrations of 2-hexene and 3-hexene, on the order of 1 ppm, were identified in some of the doped flames. The profiles of 1-pentene and 1-hexene show peaks at $z \approx 4.9$ mm. Comparison of Fig. 9 with the profiles of alkanes in Fig. 6 confirms that these olefins are formed as the fuel alkanes are decomposing. This is consistent with the well-known decomposition pathways for alkanes: H-atom abstraction or unimolecular dissociation to alkyl radicals, followed by beta-scission of the alkyl radicals to olefins and additional alkyl radicals [30]. Flames B, C, and D show good agreement in their 1-pentene profiles, with significantly larger concentrations as compared to the baseline Flame A. The agreement with respect to 1-hexene on the other hand is relatively poor, especially for Flame C. The Utah/Yale surrogate-doped flame has nearly 2.7 times as much 1-hexene as the jet fuel-doped flame, while the Aachen surrogate-doped Flame D has a peak 1-hexene

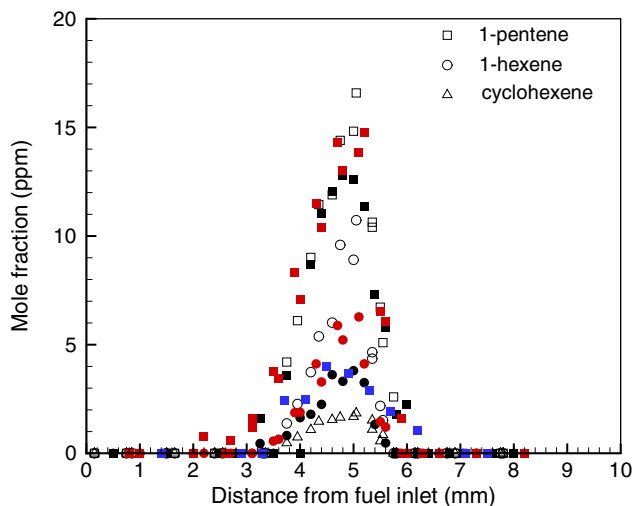


Fig. 9. Comparison of C5–C6 alkenes profiles: Flame B (full black symbols), Flame C (open symbols), Flame D (red symbols), and Flame A (blue symbols).

value almost 50% larger than that of jet fuel-doped flame. Another difference between the Aachen and Utah/Yale surrogates with respect to the formation of olefins is the presence of larger olefins. In the Aachen surrogate Flame D, about 1–2 ppm of 1-heptene and 1-octene were quantified near the peak of the C5–C6 olefins ($z \approx 4.9$ mm). On the other hand, in the Utah/Yale surrogate Flame C, only 1-octene was detected, but peaks for cyclohexene and methylcyclohexene were observed. Fig. 9 shows the profile of cyclohexene for Flame C. Analysis of the C7–C9 olefins in the jet fuel-doped Flame B is extremely difficult because of the overlapping spectra of multiple isomers. Similar challenges are posed by the quantification of dienes.

Fig. 10a shows the profiles of 1-propene for Flames A, A*, B, C, and D. The baseline ethylene flames (Flames A and A*) produce similar propene mole fractions, but the doped flames produce noticeably different propene profiles. The propene mole fraction is significantly larger than other alkenes, except obviously for the fuel species ethylene, and the peak mole fraction appears slightly after the peak of larger alkenes. The propene mole fraction peak for all three doped flames occurs at $z \approx 5.2$ mm with the highest magnitude for jet fuel (Flame B) and the lowest for the Aachen surrogate (Flame D). The difference between propene mole fraction profiles of jet fuel/surrogate-doped flames and baseline flames can be attributed to the beta-scission of large alkyl radicals all the way down

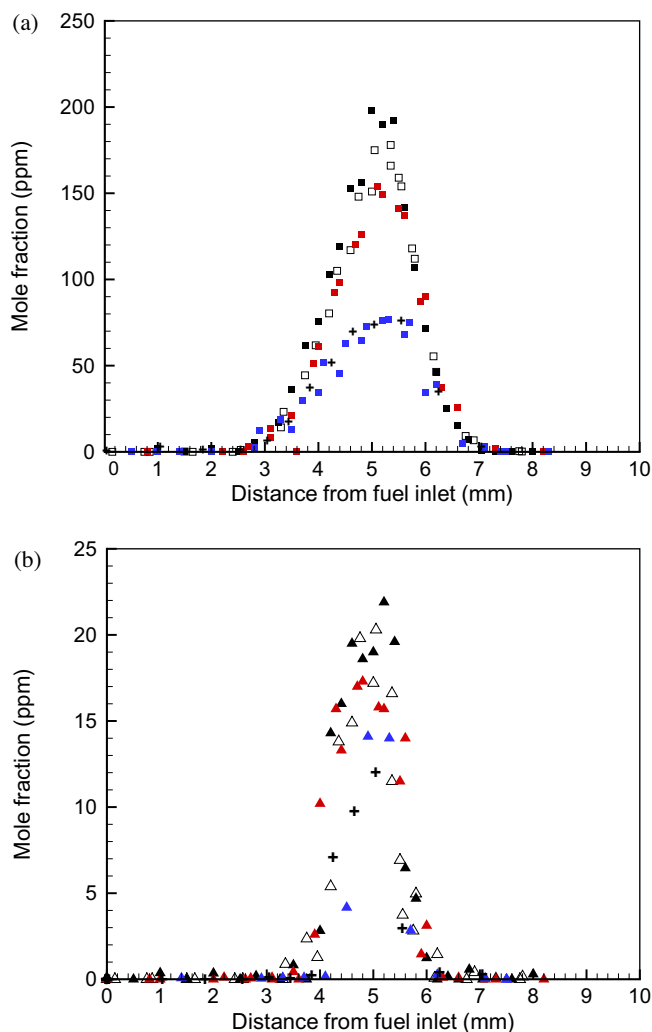


Fig. 10. Comparison of profiles of (a) 1-propene and (b) propane: Flame B (full black symbols), Flame C (open symbols), Flame D (red symbols), Flame A (blue symbols), and Flame A* (+).

to the smallest alkenes. We note that the ability of both surrogates to predict the jet fuel behavior with respect to the formation of alkenes gets better for smaller alkenes, probably because many more pathways can produce the smaller alkenes and so the specific details of the fuel alkane structure are less important.

Fig. 10b shows profiles of propane; no butane, pentane, or hexane were detected. A comparison of the location of the propane peaks with the disappearance location of the larger alkanes in Fig. 6 indicates that this small alkane is a product of the decomposition of the larger ones. The non-sooting methane flame doped with jet fuel and the Utah/Yale surrogate had almost three times as much propane as the sooting flames (Flames B and C here), which can be attributed to impurities in the methane source used in those experiments [20].

4.4. C2 hydrocarbons

Fig. 11 compares the measured C2 species in Flames A–D and Flame A*. Ethylene is a major species in the fuel stream and its trend was presented in Fig. 4. In the previous experiments on non-sooting methane flames doped with either jet fuel or the Utah/Yale surrogate, the latter overpredicted the ethylene concentrations, but accurately reproduced the ethane and acetylene concentrations [20]. Fig. 11a shows a good agreement between ethane profiles in all the incipient sooting ethylene flames. Ethane is an impurity in the fuel source, and it shows trends similar to ethylene, that is, its maximum concentration occurs at the fuel boundary, its concentration decreases throughout the flame zone, and the dopants do not make a noticeable contribution to its concentrations in the baseline flame.

Acetylene, shown in Fig. 11b, presents a unique behavior that differs in two main ways from the non-sooting methane flame. First, the peak of the acetylene profile in the sooting flames is nearly 19 times larger than the acetylene peak in the non-sooting flames, as expected in these sooting flames, since acetylene is a major surface growth species in soot formation. Second, the profiles show a multimodal behavior as evidenced by the continuous lines in the figure. At first glance this behavior may seem to be an experimental artifact. However, it is reproducible. For Flames A–D, at least two sets of experiments were conducted to confirm the reproducibility of data and this behavior was observed in all experiments. Also, if it were an artifact of the GC/MS performance or the experimental technique, we would detect multimodal behavior in other minor species such as methane or ethane with much lower absolute concentrations than acetylene, but we do not (see Figs. 5 and 11a). The results for ethane in Fig. 11a at distances less than 3 mm from the fuel inlet indicate the approximate random uncertainty in the measurements, which is 4%; the changes in the acetylene concentration due to the multimodal behavior are much larger, 20–50%. Moreover, this multimodal behavior was not observed in the non-sooting experiments using the same instrument, leading us to conclude that the acetylene participation in soot growth pathways may cause this behavior. The first drop in acetylene profiles occurs at $z \approx 3.5$ –4.5 mm. The peak of the acetylene mole fraction is at $z \approx 5.5$ –5.8 mm for all flames and the bulk of the acetylene profile occurs where ethylene is still present (ethylene disappears roughly at $z \approx 7$ mm). It is difficult to discriminate between the peak concentrations of acetylene in Flames A–D. This suggests that acetylene, which is present at very high concentrations in these flames, is mainly produced by ethylene.

Some important reactions that form single ring aromatics involve acetylene [28]. Also, acetylene is a particle surface growth species, as further discussed in the next section. The first drop in the acetylene profiles (Fig. 11b) can be attributed to the early stages of formation of benzene and other large pyrolysis products

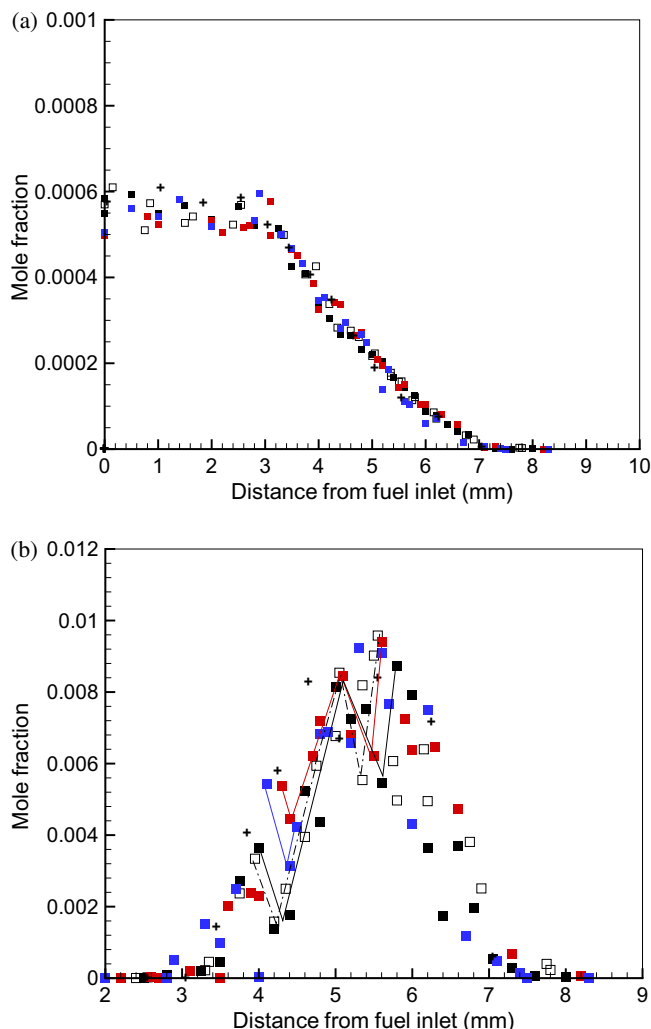


Fig. 11. Profiles of molar fractions of (a) ethane and (b) acetylene: Flame B (full black symbols), Flame C (open symbols), Flame D (red symbols), Flame A (blue symbols), and Flame A* (+). (For interpretation of the references to color in this figure legend, the reader is referred to the web version of this article.)

through reactions involving acetylene. Pyrolysis reactions of acetylene can form many products other than benzene. This drop is right before the benzene peak. The second drop may be a result of participation of acetylene in surface growth. Future studies with the use of Laser-Induced Incandescence (LII) to measure soot would confirm this hypothesis.

4.5. Aromatics

Flames A–D were deliberately selected to be at the onset of soot formation to assess the behavior of jet fuel and its surrogates with respect to the formation of critical precursors in soot formation, such as aromatics. The non-sooting methane flames doped with jet fuel and the Utah/Yale surrogate revealed significant discrepancies with respect to benzene and toluene [20], which was cause for concern in the soot context. The present study considers also the Aachen surrogate (Flame D) that was found to reproduce successfully soot volume fraction profiles of jet fuel flames [10].

Fig. 12 shows a comparison of some aromatics, namely, tetralin, *m*-xylene and 1,2,4-trimethylbenzene (TMB), among Flames B–D, with different ordinate scales in Fig. 12a and in its magnified version, Fig. 12b. None of these aromatic species were detected in the baseline ethylene flames (Flames A and A*). *p*-xylene can also be

detected and quantified in the doped flames, but it has much lower concentrations and follows a profile similar to that of *m*-xylene in Flame D. The accuracy of the tetralin calibration is uncertain and its profile is qualitative. In Flame B, tetralin, *m*-xylene, and TMB were identified and quantified. These species are considered tracers of the multitude of aromatics in the jet fuel. They decay roughly at $z \approx 5.1$ mm. In Flame C that was doped with the Utah/Yale surrogate, *m*-xylene and tetralin are the only aromatic components of the surrogate. Since these components represent a large group of aromatics in the jet fuel, the disagreement of the profiles near the fuel inlet, away from the reaction zone, is not surprising. The same consideration applies to the aromatic component of the Aachen surrogate.

In Flame D, which is doped with the Aachen surrogate, TMB is the sole aromatic compound, which decays at $z \approx 5.8$ –6 mm, which is close to where the only aliphatic compound, *n*-decane, decays. A small peak of *m*-xylene (5–6 ppm) is observed in Flame D at $z \approx 5.1$ mm, which is close to the peaks of benzene and toluene. Xylene can be formed from TMB by chemical pathways that replace a methyl side-chain with an H atom. Very small quantities of styrene were detected within $z \approx 3.6$ –5.1 mm, but no detectable tetralin and naphthalene were found in Flame D. Also, styrene and

naphthalene (not shown here) were detected in Flame C, within the regions of $z \approx 3.3$ –5 mm and $z \approx 1.6$ –4 mm, respectively. Naphthalene could not be measured closer to the reaction zone because its GC/MS retention time is too close to that of dodecane. No naphthalene and styrene could be measured anywhere in the jet fuel flame (Flame B) because of the difficulty in species separation for jet fuel.

The two aromatic compounds that could be measured cleanly in all of the doped flames, and therefore that could be used as tracers of aromatics and soot formation, are benzene and toluene. Fig. 13 illustrates how these compounds are related to the formation of the two-ring aromatic naphthalene, which is a critical bottleneck to soot formation. Benzene is an intermediate in the growth of aliphatics (e.g., methylcyclohexane, iso-octane, and dodecane) to naphthalene, and toluene is a byproduct of the growth of *n*-alkylbenzenes to naphthalene via benzyl radical. We focus on toluene instead of benzyl radical because we cannot detect radicals.

A comparison for benzene and toluene among the various flames is shown in Figs. 14 and 15, respectively. Significantly, even in the case of the jet fuel (Flame B), whose chromatograms are the most difficult to analyze, benzene and toluene can be measured with small uncertainties, since they do not have multiple isomers and they appear early in the chromatogram, before the time when the “grassy” baseline arises (see Fig. 7). In fact, the GC/MS has a better performance in separating the jet fuel intermediate species as z increases and the large fuel compounds and their isomers are pyrolyzed and partially oxidized. Indeed, the profiles of carbon count in Fig. 8 suggest that beyond $z \approx 5.3$ mm, the total carbon counts are consistent between Flames B, C, and D and the comparison is quantitative. This region is in the vicinity of peaks of benzene and toluene mole fractions.

Fig. 14 shows good agreement between the surrogates and jet fuel with respect to the location and magnitude of the benzene mole fraction peak. The doped flames produce much more benzene than the two baseline ethylene flames (A and A*), which means that maximum concentrations in the doped flames reflect aromatics formation from the dopants. The agreement is better for Flame C (Utah/Yale surrogate) than for Flame D (Aachen surrogate). Although the benzene profiles in the Aachen surrogate flame (Flame D) and the jet fuel flame (Flame B) follow similar trends, the Aachen surrogate produces nearly 20% less benzene than jet fuel. The sooting jet fuel-doped Flame B produces nearly 2.5 times more benzene than the non-sooting jet fuel-doped methane flame [20].

Comparison of toluene mole fractions in Fig. 15 shows reasonably good agreement between Flame B and Flame C. Small amounts of toluene are present in the parent jet fuel causing the

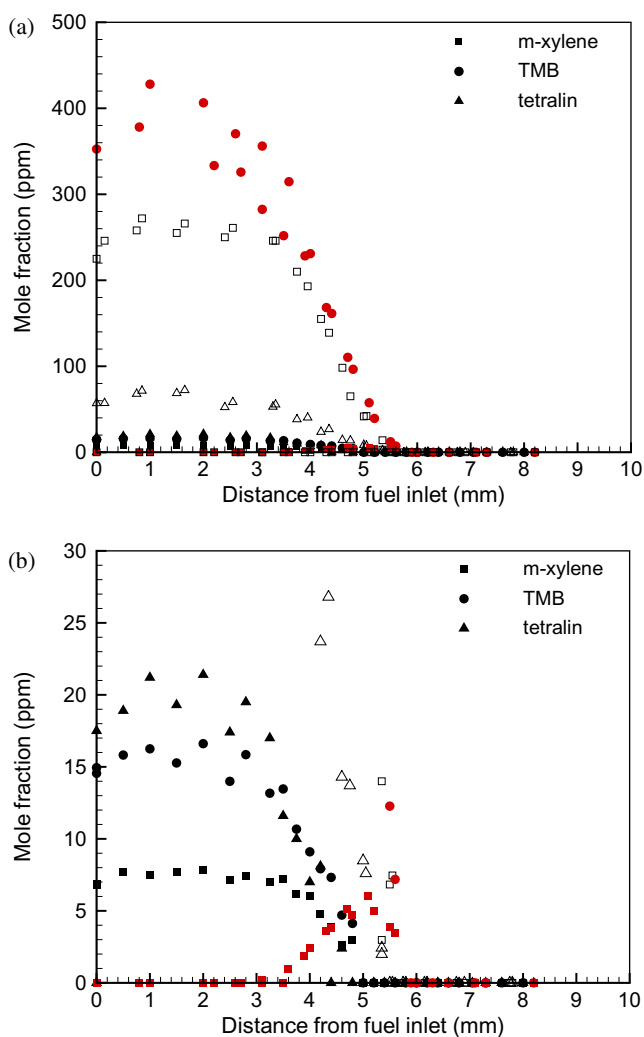


Fig. 12. Comparison of profiles of *m*-xylene, tetralin, and 1,2,4-trimethylbenzene with compressed (a) and expanded (b) ordinate scales: Flame B (full black symbols), Flame C (open symbols), and Flame D (red symbols). (For interpretation of the references to color in this figure legend, the reader is referred to the web version of this article.)

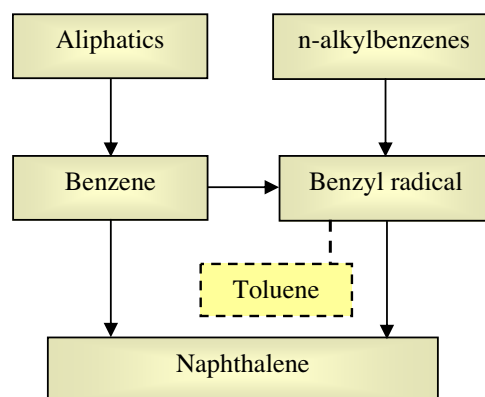


Fig. 13. Global pathways of naphthalene formation.

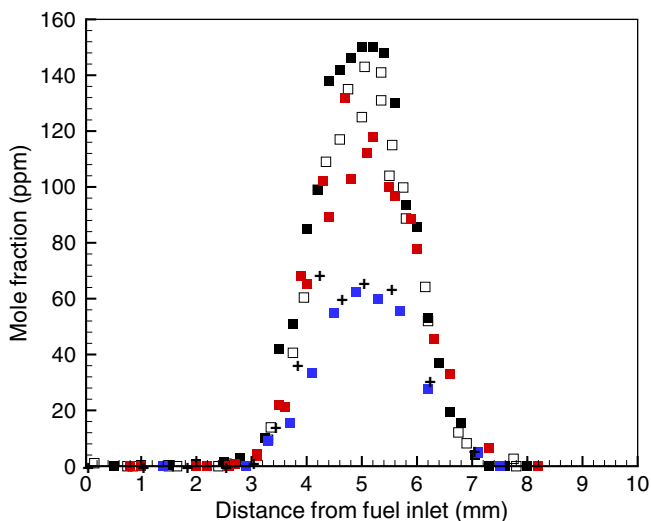


Fig. 14. Comparison of profiles of benzene mole fractions: Flame B (full black symbols), Flame C (open symbols), Flame D (red symbols), Flame A (blue symbols), and Flame A* (+). (For interpretation of the references to color in this figure legend, the reader is referred to the web version of this article.)

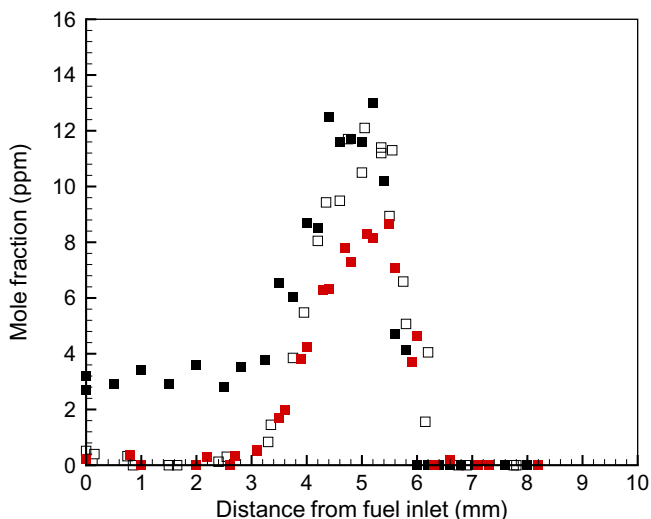


Fig. 15. Comparison of profiles of toluene mole fractions: Flame B (full black symbols), Flame C (open symbols), and Flame D (red symbols). (For interpretation of the references to color in this figure legend, the reader is referred to the web version of this article.)

mole fractions to be non-zero for small values of z . Toluene was not detectable in Flames A and A*. The much larger toluene/benzene ratios in the doped flames versus the undoped flames indicate that the toluene in the doped flames is primarily formed from the aromatic components of the jet fuel and surrogates independently of benzene formation. The agreement between Flame B and Flame D is also reasonable, with nearly similar peak location, but the peak magnitude is almost 30% smaller in Flame D. These observations suggest that, despite its simplicity, the Aachen surrogate has an acceptable agreement with jet fuel in incipient sooting conditions with respect to aromatic formation.

In summary, it would appear that the discrepancies between jet fuel and surrogates that were observed under non-sooting conditions [20] are not present in the current, and more relevant, situation of incipient sooting.

The focus of this study is not on the final stages of soot formation. Instead, we considered the decomposition and oxidation of fuels leading to the formation of small aromatics that are important since they grow eventually to soot. To study the sooting tendency of surrogate fuels, Yang et al. [37] used the threshold sooting index (TSI) [38]. The TSI of the jet fuel is somewhat uncertain since its composition varies, but values in the literature range from 15 to 26 [39]. We have calculated the TSI of the Utah/Yale and Aachen surrogates using the mixing rule, $TSI_{mix} = \sum x_i TSI_i$ [37], where x_i is the mole fraction of the individual components. TSI values for pure hydrocarbons are obtained from the work of Olson et al. [40]. The TSI of the Utah/Yale surrogate, which contains 13.4 (liq.) vol% aromatics, is 14.6, while that of the Aachen surrogate which contains 17.2 (liq.) vol% aromatics, is 15.1. Aromatics account for roughly 18 vol% of jet fuel [34]. By consideration of this global measure of sooting tendency one would expect a tentative trend for soot formation: jet fuel > Aachen surrogate > Utah/Yale surrogate.

4.5.1. Possible role of the antistatic additive

A final issue to consider is the influence of trace amounts of sulfur compounds in jet fuel (about 490 ppm) on the formation of soot precursors. The sulfur trioxide reaction $H + SO_3 \rightarrow OH + SO_2$, in the late pyrolysis process of diffusion flames forms the hydroxyl radical that attacks soot precursors and suppresses soot formation [30]. The good agreement in aromatics behavior and the similarity of flame appearance under incipient sooting conditions suggest that the presence of sulfur in the parent liquid plays a negligible role. However, the situation is more complex in the present experiments relying on the electro-spray for fuel dispersion. The electro-spray can operate successfully so long as the fluid has a finite electric conductivity, which is not the case for hydrocarbons. Consequently, we need to add 0.05% (by volume) of an antistatic additive, Octel Stadis 450, to elevate the liquid electrical conductivity. This additive is also present in some jet fuels as a static dissipater for in-flight refueling, at concentrations not exceeding 80 ppm. It contains up to 30% in sulfur compounds [34,41], which corresponds to a maximum of 0.018% (by weight) in a surrogate mixture. To ascertain if the additive played any role, we performed the following experiment: we selected a flame with boundary conditions similar to Flame B except for the dopant that was jet fuel at 3000 ppm, to ensure a more pronounced soot-laden zone. In a separate experiment, the liquid fuel was spiked with 4-dodecylbenzene sulfonic acid, yielding a fivefold increase in the sulfur contribution as compared to that from the Stadis. No distinct changes in the soot zone luminosity (see Fig. 2) and thickness were observed, which suggests that the observed trends in terms of soot and soot precursors are not an artifact associated with the antistatic additive.

5. Conclusions

A well-defined baseline ethylene flame under incipient sooting conditions was perturbed with the addition of 2000 ppm by mole of either jet fuel or two surrogates, a six-component Utah/Yale blend and a two-component Aachen surrogate. The similarity in profiles of temperature, major species, and one minor species in all flames lends credence to the use of this perturbation approach to treat the flame as a flow reactor, with virtually identical conditions, except, of course, for the imposed perturbation. Principal conclusions follow:

- The data for C7–C12 alkanes are consistent with typical decomposition of large alkanes with both surrogates showing a reasonably good qualitative agreement with jet fuel in their pyrolysis

trends. More quantitative agreement is difficult to achieve, because of the complex chromatograms of jet fuel with overlapping peaks due to isomerism.

- Olefins are formed as the fuel alkanes decompose. Both jet fuel and surrogate doped flames show good agreement in their 1-pentene profiles. The agreement with respect to 1-hexene, on the other hand is relatively poor, with the Utah/Yale surrogate-doped flame and the Aachen surrogate-doped flame having concentrations a factor of 2.7 and almost 1.5 larger than jet fuel-doped flame, respectively. The agreement improves for smaller alkenes, such as propene, probably because the specific details of the fuel alkane structure are less important since many pathways can produce the smaller intermediates.
- The concern in terms of significant aromatics discrepancy between jet fuel and one of the surrogates that was reported for non-sooting flames in a previous study are not applicable in the present, and more relevant, situation of incipient sooting. In fact, good agreement was found between the jet fuel-doped and the surrogate-doped flames with respect to the location and magnitude of the benzene mole fraction peak, with the Aachen surrogate performing slightly worse and producing about 20% less benzene than the others. Comparison of toluene mole fractions shows also reasonably good agreement between flames, with the Aachen surrogate still underperforming and underpredicting the peak magnitude by almost 30%. Nevertheless, the somewhat worse, but still adequate, performance of the Aachen surrogate is compensated by its simplicity, since it consists of only two components as compared to the six components of the Utah/Yale surrogate.
- Acetylene presents a unique behavior with peak concentrations nearly 19 times larger than in the previously studied non-sooting flames, as expected, since acetylene is a major contributor to soot formation. Furthermore, the profiles show a multimodal behavior, with a first local minimum that may be attributable to acetylene participation in the formation of soot precursors such as benzene and other large pyrolysis products, and a subsequent local minimum, which may be the result of its participation in surface growth of soot particles.

Acknowledgments

The authors gratefully acknowledge: the financial support of AFOSR (Grant #FA9550-06-1-0018, Dr. Julian Tishkoff, Program Manager); the supply of jet fuel from Dr. James (Tim) Edwards (Wright-Patterson Air Force Base); the technical assistance of Mr. Hugo Bufferand who performed preliminary experiments on these flames; and the help of Mr. N. Bernardo in the construction of the hardware.

References

- [1] T. Edwards, L.Q. Maurice, J. Propul. Power 17 (2) (2001) 461–466.
- [2] M. Colket, T. Edwards, S. Williams, N.P. Cernansky, D.L. Miller, F. Egolfopoulos, P. Lindstedt, K. Seshadri, F.L. Dryer, C.K. Law, D. Friend, D.B. Lenhart, H. Pitsch,

- A. Sarofim, M. Smooke, W. Tsang, in: 45th AIAA Aerospace Sci. Meet. Exhibit, 2007, Paper No. AIAA2007-0770.
- [3] P. Dagaut, M. Cathonnet, Prog. Energy Combust. Sci. 32 (2006) 48–92.
- [4] C.P. Wood, V.G. McDonnell, R.A. Smith, G.S. Samuelson, J. Propul. Power 5 (4) (1989) 399–405.
- [5] W.D. Schulz, ACS Petrol. Chem. Div. Preprints 37 (2) (1991) 383–392.
- [6] A. Violi, E.G. Eddings, A.F. Sarofim, S. Granata, T. Faravelli, E. Ranzi, Combust. Sci. Technol. 174 (2002) 399–417.
- [7] A. Agosta, N.P. Cernansky, D.L. Miller, T. Faravelli, E. Ranzi, Exp. Therm. Fluid Sci. 28 (2004) 701–708.
- [8] C.J. Montgomery, S.M. Cannon, M.A. Mawid, B. Sekar, in: 40th AIAA Aerospace Sci. Meet. Exhibit, 2002, Paper No. AIAA 2002-0336.
- [9] S. Humer, A. Frassoldati, S. Granata, T. Faravelli, E. Ranzi, R. Seiser, K. Seshadri, Proc. Combust. Inst. 31 (2007) 393–400.
- [10] S. Honnet, K. Seshadri, U. Niemann, N. Peters, Proc. Combust. Inst. 32 (2009) 485–492.
- [11] R.H. Natelson, M. Kurman, N.P. Cernansky, D.L. Miller, Fuel 87 (10–11) (2008) 2339–2342.
- [12] A.T. Holley, Y. Dong, M.G. Andac, F.N. Egolfopoulos, T. Edwards, Proc. Combust. Inst. 31 (2007) 1205–1213.
- [13] S.S. Vasu, D.F. Davidson, R.K. Hanson, Combust. Flame 152 (2008) 125–143.
- [14] E. Ranzi. Available from: <<http://www.chem.polimi.it/CRECKModeling/kinetic.html>>, 2006.
- [15] H.R. Zhang, E.G. Eddings, A.F. Sarofim, Proc. Combust. Inst. 31 (2007) 401–409.
- [16] S.S. Vasu, D.F. Davidson, Z. Hong, V. Vasudevan, R.K. Hanson, Proc. Combust. Inst. 32 (2009) 173–180.
- [17] S.S. Vasu, D.F. Davidson, R.K. Hanson, Combust. Flame 156 (2009) 736–749.
- [18] J.A. Cooke, M. Bellucci, M.D. Smooke, A. Gomez, A. Violi, T. Faravelli, E. Ranzi, Proc. Combust. Inst. 30 (2005) 439–446.
- [19] L. Tosatto, B.L. Mantia, H. Bufferand, P. Duchaine, A. Gomez, Proc. Combust. Inst. 32 (2009) 1319–1326.
- [20] H. Bufferand, L. Tosatto, B.L. Mantia, M.D. Smooke, A. Gomez, Combust. Flame 156 (2009) 1594–1603.
- [21] G. Bikas, Kinetic Mechanisms for Hydrocarbon Ignition, Doktor der Ingenieurwissenschaften thesis, RWTH Aachen University, Fakultät für Maschinenwesen, 2001. Available from: <<http://deposit.dbb.de/cgi-bin/dokserv?idn=964932857>>.
- [22] E. Ranzi, M. Dente, G. Bozzano, A. Goldaniga, T. Faravelli, Prog. Energy Combust. Sci. 27 (2001) 99–139.
- [23] M.H. DUBY, W. Deng, K. Kim, T. Gomez, A. Gomez, J. Aerosol Sci. 37 (2006) 306–322.
- [24] C. Shaddix, K. Brezinsky, I. Glassman, Proc. Combust. Inst. 24 (1992) 683–690.
- [25] R.G. Butler, I. Glassman, Proc. Combust. Inst. 32 (2009) 395–402.
- [26] A. Hamins, D.T. Anderson, J.H. Miller, Combust. Sci. Technol. 71 (1990) 175–195.
- [27] C.S. McEnally, L.D. Pfefferle, Combust. Sci. Technol. 131 (1998) 323–344.
- [28] C.S. McEnally, L.D. Pfefferle, B. Atakan, K. Kohse-Höinghaus, Prog. Energy Combust. Sci. 32 (2006) 247–294.
- [29] K. Seshadri, F.A. Williams, Int. J. Heat Mass Transfer 21 (1978) 251–253.
- [30] I. Glassman, Combustion, third ed., Academic Press, 1996.
- [31] A. Gomez, G. Sidebotham, I. Glassman, Combust. Flame 58 (1984) 45–57.
- [32] R.L. Axelbaum, W.L. Flower, C.K. Law, Combust. Sci. Technol. 61 (1–3) (1988) 51–73.
- [33] B.M. Kumfer, S.A. Skeen, R.L. Axelbaum, Combust. Flame 154 (2008) 546–556.
- [34] T. Edwards, J. Propul. Power 19 (6) (2003) 1089–1107.
- [35] D.C. Rapp, Ph.D. thesis, Pennsylvania State University, PA, 1996.
- [36] B.A.V. Bennett, C.S. McEnally, L.D. Pfefferle, M.D. Smooke, M.B. Colket, Combust. Flame 127 (1–2) (2001) 2004–2022.
- [37] Y. Yang, A.L. Boehman, R.J. Santoro, Combust. Flame 149 (2007) 191–205.
- [38] H.F. Calcote, D.M. Manos, Combust. Flame 49 (1983) 289–304.
- [39] Z. Yang, M. Chaos, F.L. Dryer, 2006, Surrogate Composition Effects: A Comparison of Surrogate Mixture Candidates with Combustion Targets (H/C, TSI, CN), presented at the Surrogate Fuels Working Group Meeting, January 6th, 2008, Reno, Nevada. Available from: MURI website.
- [40] D.B. Olson, J.C. Pickens, R.J. Gill, Combust. Flame 62 (1985) 43–60.
- [41] C.P. Henry, Enhanced Antistatic Additives for Hydrocarbon Fuels and Solvents, US Patent No. US2007/0220803 A1, 2007.